Solid-Phase Speciation of Pb in Urban Road Dust Sediment: A XANES and EXAFS Study

JUDITH E. S. BARRETT,[†] KEVIN G. TAYLOR,*[,†] KAREN A. HUDSON-EDWARDS,[‡] AND JOHN M. CHARNOCK[§]

Department of Environmental and Geographical Sciences, Manchester Metropolitan University, Manchester M15 6BH, U.K., Department of Earth and Planetary Sciences, Birkbeck, University of London, Malet St., London WC1E 7HX, U.K., and School of Earth, Atmospheric and Environmental Sciences, University of Manchester, Manchester, M13 9PL, U.K.

Received December 10, 2009. Revised manuscript received March 11, 2010. Accepted March 11, 2010.

The quality of the urban environment is of growing concern as its human population continues to dramatically increase. X-ray absorption spectroscopy (XAS) and SEM have been used to study the solid-phase speciation of Pb in urban road dust sediments (RDS) in Manchester, UK. XANES analysis and linear combination modeling indicate that $PbCrO_4$ and Pb-sorbed goethite occur in 1000−500 μm, 250−125 μm, 63−38 μm, and <38 μm size fractions, collectively representing between 51−67% of the contributing Pb-phases. XANES analysis suggests that PbO, $PbCl_2$, and Pb carbonates are also present. EXAFS modeling for all grain size fractions gives best fit models with a first shell of two oxygen atoms at 2.29−2.32 Å, which corroborate the possible presence of Pb-sorbed goethite, and also suggest the presence of Pb phosphates and Pb oxides. Second shell Pb−Fe and second and third shell Pb−Pb scattering distances confirm Pb-sorbed to Fe oxide, and $PbCl_2$ and $PbCrO_4$, respectively. Many of the XAS models are corroborated by SEM observations. The Pb-phases may pose a risk to human health if inhaled or ingested, with insoluble phases such as $PbCrO_4$ potentially causing inflammation in the lungs, and soluble phases such as PbO potentially being the most bioaccessible in the digestive tract.

Introduction

Over 50% of the global population currently lives in urban areas (*1*), a figure set to increase considerably over the coming decades. Therefore, the quality of urban environments is a matter of global concern. Accumulations of particulates on road surfaces (referred to here as road dust sediment, RDS) are major sources of both water-borne and atmospheric particulates in urban environments and are commonly highly contaminated by metallic elements such as Pb (*2*). Lead is highly toxic to humans, with excessive intake causing anemia and diseases of the kidneys, heart, immune, nervous, reproductive, and gastrointestinal systems (*3*). Humans are exposed to Pb through natural and anthropogenic pathways that include RDS.

* Corresponding author e-mail: k.g.taylor@mmu.ac.uk.
[†] Manchester Metropolitan University.
[‡] University of London.
[§] University of Manchester.

Although RDS is often highly enriched in Pb (*2, 4*), few studies have been carried out to investigate its solid-phase speciation. Duggan and Williams (1977) used chemical extraction methods (dilute hydrochloric acid) to estimate the bioavailibility of Pb in RDS within Greater London (*4*). Biggins and Harrison (1980) used X-ray diffraction (XRD) to investigate RDS, and identified six crystalline Pb species, including $PbSO_4$ (*5*). They concluded, however, that as crystalline compounds only accounted for a small percentage of the total Pb there was a need to seek alternative techniques to more thoroughly understand the solid-phase Pb speciation. Such an understanding would also enable better estimates of the bioavailability of Pb in RDS to be made, since this is related to the stability and solubility of the Pb species.

Numerous studies have demonstrated that a synergistic approach that combines many mineralogical and spectroscopic techniques is highly effective for characterizing the solid-phase speciation of metallic elements in environmental materials such as soils, dredged sediment, and soils (*6, 7*). Techniques such as X-ray diffraction, transmission and scanning electron microscopy, and especially, X-ray absorption near-edge structure (XANES) and extended X-ray absorption fine structure (EXAFS) spectroscopies are used to give information about the composition, crystallinity, and bonding environments of the metallic elements and their hosts. In this paper, we use such an approach to characterize the solid-phase speciation of Pb in RDS from a well-used urban road in Manchester, a major city in NW England.

Experimental Methods

RDS was collected from Oxford Road, situated within the university area of the City of Manchester, in November 2004, four years after leaded-petrol was banned in the UK. It is an anthropogenically active site, with a residual population amplified daily and seasonally by commuters, students, and visitors. In the preliminary stages of this research, the chemical composition of RDS from the Oxford Road site over a transect of 550 m was characterized, and rigorous statistical analysis of these data reveal no significant compositional variability (Barrett, unpublished data). Hence, one statistically representative sample site (British national Grid Reference: SJ843973) was selected for the in-depth analysis reported here (limitations on synchrotron beamtime dictated this approach). A 10 kg RDS sample was collected from a traffic island site using a plastic dust pan and brush, as recommended by Charlesworth and Lees (*8*). Due to the large accumulation of RDS at this site, and the ability to sample coherent agglomerations, we believe that any loss of fines was minimal.

The sample was air-dried in soil bags at an average temperature of 21 °C. Constant mass was attained after 14 days. Ten percent of the dried bulk sediment sample was retained as an archive. A meshed sieve was used to remove material ≥2000 μm from the remaining sediment sample. The ≤2000 μm sediment sample was then dry sieved into seven grain size fractions using standard sieve methods (see Supporting Information (SI) Table S1 for mass fractions by grainsize). Recovery of sediment was determined to be 99.5%. Storage and handling of all sediments samples was carried out in such a way as to minimize atmospheric contamination.

Pseudototal Pb concentrations in each grain-size fraction were estimated using open-vessel digestion in aqua-regia at 85 °C for 2 h. To allow for the inhomogeneous character of RDS 6 replicas of 0.5 ± 0.02 g per grain size fraction were digested. Resulting solutions were analyzed for Pb and 18

10.1021/es903737k

other elements using a Varian Vista AX CCD simultaneous ICP-OES with echelle optics, with aqua-regia as matrix and rinse agent (see SI Table S2 for full data). The number of reagent blanks was set at 10% of the total number of samples. Certified reference material LGC6139 (certified for aqua-regia) was digested and analyzed to determine the reliability of the method. The precision, estimated through the coefficient of variance, and trueness, estimated by bias analysis, were determined to be 7.9% and −1.8% ($n = 19$) for Pb, respectively. The pseudototal median Pb concentrations and mass loadings (in brackets; means of six replicates) for the four grain size fractions analyzed by XAS (1000−500 μm, 250−125 μm, 63−38 μm, and <38 μm) are 41.4 μg g^{-1} (5%), 72 μg g^{-1} (31%), 280 μg g^{-1} (11%), and 380 μg g^{-1} (10%), respectively (see SI Table S1 for full data).

For scanning electron microscopy analysis of grains within the RDS, subsamples of each grain size fraction were mounted in epoxy resin in a vacuum oven, cured, cut, and polished with diamond paste, and carbon coated. Observations were made with a Jeol 6400 SEM equipped with a backscattered electron detector. The microscope was operated at 20 kV, 2 nA and at a working distance of 15 mm. The presence of Pb-bearing grains was determined qualitatively using an energy dispersive X-ray microanalysis (EDAX) system. X-ray diffraction analysis on both untreated and heavy-liquid concentrated subsamples of each grain-size fraction was undertaken using a Philips X-Pert PW3719 diffractometer with Cu Kα radiation. Mineral identification was based on 2θ peak positions. No quantification was undertaken.

Four grain size fractions (1000−500 μm, 250−125 μm, 63−38 μm, and <38 μm; this limit dictated by beamtime constraints) were selected for X-ray absorption spectroscopy to represent street dust material that remains on street surfaces or is removed by sweeping (the coarsest two fractions), and those fractions most readily entrained in water (63−38 μm) and air (<38 μm). X-ray absorption near-edge structure (XANES) and extended X-ray absorption fine structure (EXAFS) spectroscopies were used to determine the local bonding environment of Pb in the RDS. For bulk analysis, X-ray absorption spectra at the Pb L_{III}-edge were collected using air-dried unground samples of each of the grain-size fractions that were mounted in aluminum holders, on station 16.5 at CCLRC Daresbury synchrotron radiation source. Operating conditions were 2 GeV with an average current of 140 mA, and a vertically focusing mirror and a sagitally bent focusing Si(220) double crystal monochromator detuned to 80% transmission were used to minimize harmonic contamination. Data were collected in fluorescence mode using an Ortec 30 element solid state Ge detector. Experiments were performed at ambient temperature, averaging multiple scans for each sample (8−24 depending on Pb concentration). X-ray absorption spectra were also collected in fluorescence mode for Pb-sorbed goethite, and in transmission mode (double scan) at the Pb L_{III}-edge for a suite of Pb model compounds ($PbCrO_4$, PbO-orthorhombic, $(PbCO_3)_2.Pb(OH)_2$, $PbSO_4$, $PbCl_2$, $Pb_5[Cl(PO_4)_3]$, $PbNO_3$, $Pb(C_2H_3O_2)_2$) to allow comparison with experimental data for the natural samples. With the exception of Pb-sorbed goethite, the model compounds were chemical standards of 98% purity or greater. Goethite was synthesized in the laboratory and Pb sorbed to it using standard published methods (*9*). Model compounds were selected to include those previously suggested as important Pb-species within either RDS or contaminated soils and sediments (*15, 10, 11*).

XANES data were fitted using a linear combination of XANES spectra collected from the model systems. For this study the contribution of individual compounds in a best fit linear combination is considered to be correct to within ±5% of the total metal content. However, the level of uncertainty may be affected by inhomogeneities in the samples as well as the signal-to-noise ratio (*12*). The combination of low signal-to-noise ratio that characterizes the Pb experimental XANES spectra and the inherent heterogeneity of RDS matrix are likely to result in an estimated error that is greater than ±5% of the total metal content quoted. Therefore, we place less confidence in individual contributions of reference compounds determined to be <10% of the total Pb content.

Background-subtracted EXAFS spectra were analyzed in EXCURV98 using full curved wave theory (*13, 14*). Phaseshifts were derived in the program from ab initio calculations using Hedin-Lundqvist potentials and von Barth ground states (*15*). Fourier transforms of the EXAFS spectra were used to obtain an approximate radial distribution function around the central Pb atoms (the absorber atoms); the peaks of the Fourier transform can be related to "shells" of surrounding back scattering atoms characterized by atom type, number of atoms in the shell, the absorber-scatterer distance, and the Debye−Waller factor, $2\sigma^2$ (a measure of both the thermal motion between the absorber and scatterer and of the static disorder or range of absorber−scatterer distances). The data were fitted for each sample by defining a theoretical model and comparing the calculated EXAFS spectrum with the experimental data. Shells of backscatterers were added around Pb and by refining an energy correction E_f (the Fermi energy), the absorber−scatterer distance, and Debye−Waller factor for each shell, a least-squares residual (the *R*-factor, ref *16*) was minimized. The statistical significance of each added shell was tested using a reduced chi-squared test.

Results and Discussion

SEM and XRD Observations. Iron-oxide grains were identified by SEM in all four grain-size fractions (Figure 1a) and are similar to Pb-bearing iron oxides using electron microprobe analysis on other RDS materials (*17*). In addition, Pb- and Cr-bearing grains were noted in the <38 μm fraction (Figure 1b), and Pb in association with P (Figure 1c) and in association with Cl (Figure 1d) was noted in the 63−38 μm and 250−125 μm fractions, respectively. XRD traces show that quartz is the dominant crystalline phase all in grain-size fractions. Iron oxide (hematite or magnetite), calcite and felspathic minerals (albite and microcline) are a minor component in all size fractions, and the phyllosilicates kaolinite and chlorite are also minor phases in the 63−38 μm and <38 μm fractions. Trace amounts of anglesite ($PbSO_4$), Pb-apatite, Pb basic carbonate and Pb oxide chloride are indicated by the XRD data for the heavy mineral separate fractions from all grain fractions (with the exception of the <38 μm fraction), and this is consistent with other published data for RDS (*5*).

X-ray Absorption near Edge Structure (XANES) and Linear Combination Fitting. The Pb-L_{III}-edge XANES spectra for the four grain-size fractions of the Manchester RDS and the selected Pb reference compounds are shown in Figure 2. The four experimental spectra are similar in profile, phase and amplitude, with edge crests occurring between 13 057 and 13 060 eV. Additionally, a broad high energy peak between 13 080 and 13 120 eV is observed in each of the four spectra. Careful scrutiny of the 250−125 μm, 63−38 μm, and <38 μm spectra suggests the presence of weak shoulder structures and edge peaks. The high noise evident in the 1000−500 μm grain-size spectrum means that the discrimination of similar edge structures is severely restricted.

The Pb-L_{III}-edge XANES spectra of Pb(II) compounds are known to be sensitive to the first-shell coordination environments, with clear differences in the XANES spectra arising from slight variations in the level of distortion and number of oxygen in the first shell of Pb(II) complex (*18, 19*). Therefore, the similarity of the four experimental spectra suggests, with respect to Pb(II) compounds, that the first neighbor coordination environments are similar. Edge width and line shape

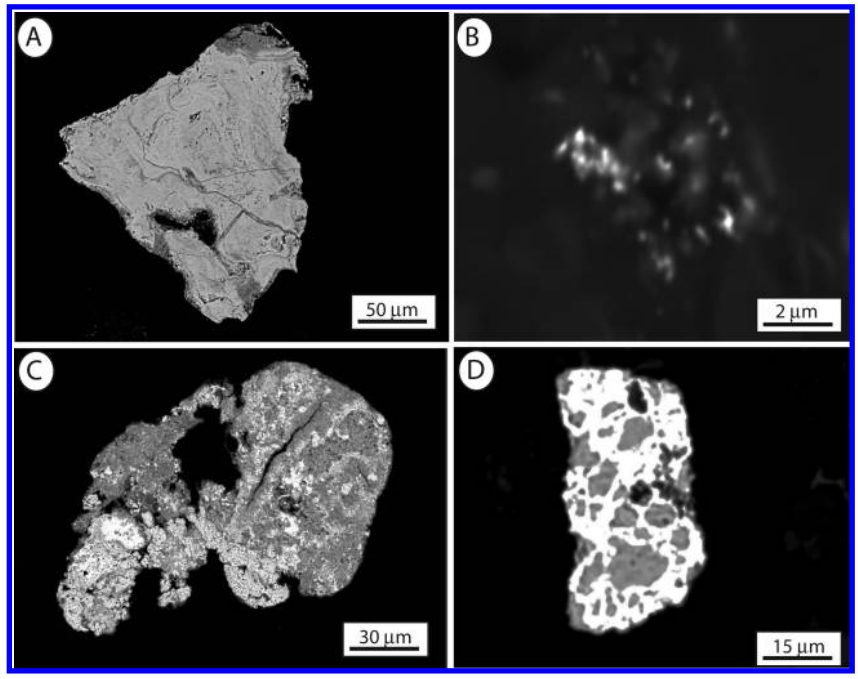

FIGURE 1. Backscatter electron images of grain types associated with Pb within the Manchester RDS. (A) Iron oxide grain (250−125 μm fraction). (B) Pb- and Cr-rich particles (bright areas) (<38 μm fraction). (C) Pb- and P-rich grain (bright area) (63−38 μm fraction). (D) Pb- and Cl-rich grain (250−125 μm fraction).

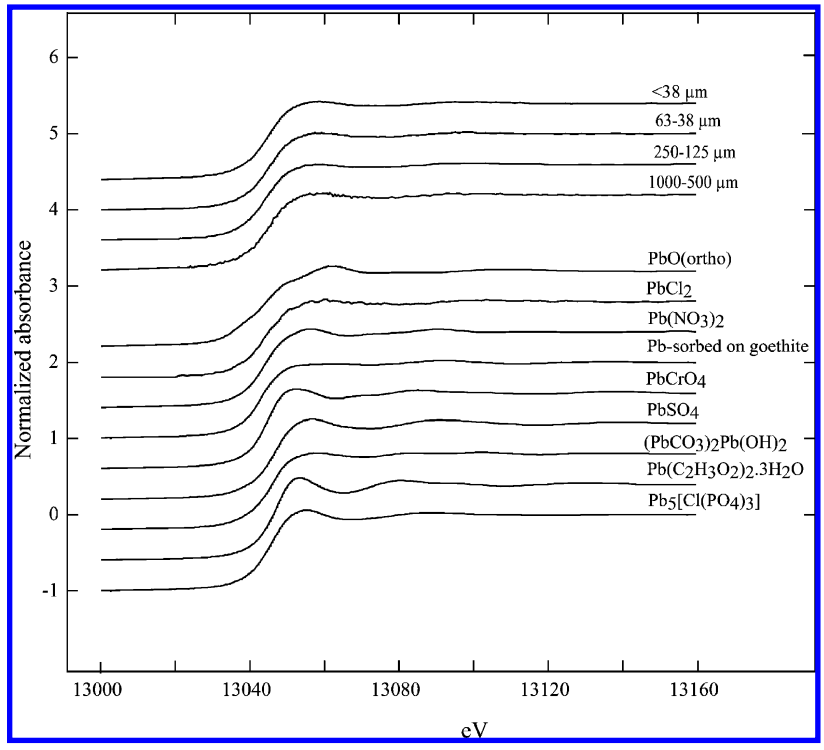

FIGURE 2. Experimental Pb-L_{III}-edge XANES spectra of the four grain-specific fractions and for the nine model compounds used in the best fit linear combination analysis.

are influenced by the symmetry of the Pb site and the dominance of covalent bonding in the Pb complex, with a tendency for edge widths to be narrower for Pb sites characterized by high point group symmetry (*20*). The general shape and width of edge of the experimental spectra (Figure 2) suggests that the symmetry of Pb complexes in the Manchester RDS is not significantly influenced by Pb(II) sites with high symmetry. Equally, the broad shape may reflect covalent bonding in Pb compounds in the RDS matrix. Differences in edge widths noted between individual grain-size spectra are likely to arise due to subtle differences in the symmetry of Pb(II) sites and the degree of covalency exhibited by Pb complexes.

The XANES linear combination best fits are reported in Table 1. These suggest that Pb in Manchester RDS is complexed predominately to inorganic ligands. It is only in the finest fraction that organic ligands, in the form of Pb acetate, appear to make a contribution (13.4%). Lead-sorbed goethite (24−51%) is found in all grain-size fractions, and is the dominant Pb phase in the three finest fractions. XANES fitting suggests that $PbCrO_4$ (9−34%) is also common to all grain-size fractions. $PbO_{(ortho)}$ is identified as a major

TABLE 1. Summary of the Percentage Contributions of Model Compounds Using Best Fit Linear Combination Analysis for the 1000−500 μm, 250−125 μm, 63−38 μm, and <38 μm Grain-Size Fractions of the Manchester RDS Samples[a]

grain-size (μm)	Pb-goethite	$PbCrO_4$	PbO (orthorhombic)	$(PbCO_3)_2$. $Pb(OH)_2$	$PbSO_4$	$PbCL_2$	$Pb_5[Cl(PO_4)_3]$	$PbNO_3$	$Pb(C_2H_3O_2)_2$	R (%) χ^2
1000−500	24.1	34.1	29.8	0	12.0	0	0	0	0	0.051 (0.022)
250−125	42.5	9.3	0	11.1	0	30.4	6.8	0	0	0.015 (0.007)
63−38	51.0	15.8	0	33.1	0	0	0	0	0	0.015 (0.007)
<38	44.9	21.1	12.9	0	7.7	0	0	0	13.4	0.011 (0.005)

[a] Note: R (%) is the comparative goodness of fit. χ^2 is the measure of the absolute goodness of fit.

component of the theoretical XANES fit for the 1000−500 μm spectrum, but makes little to no contribution to the fitting of the 250−125 μm, 63−38 μm and <38 μm experimental spectra. Lead basic carbonate ($(PbCO_3)_2.Pb(OH)_2$) only contributes to the fit of the 63−38 μm grain size fraction (33%) and to a lesser extent in the 250−125 μm grain-size fraction (11%). Lead sulfate is only a component in the coarsest and finest fractions, where its contribution to the XANES fit is ≤12%. $Pb_5[Cl(PO_4)_3]$ contributes uniquely to the fitting of the 250−125 μm fraction, although only as a minor component. $PbCl_2$ makes a considerable contribution to the fit of the 250−125 μm grain-size fraction (30%).

The possible absence of reference compound spectra leading to the misidentification of components in the experimental sample (*11, 12*) cannot be ruled out. However, the confirmation of the presence of the modeled species through SEM observations adds to the confidence in the interpretation.

Extended X-ray Absorption Fine Edge Structure (EXAFS). Figure 3 shows k^3-weighted EXAFS Pb L_{III}-edge spectra and fits with the corresponding Fourier transforms (FTs) for the best statistically justified fit for the four grain-size fractions. The FTs for all the grain-size fractions (Figure 3 e−h) are dominated by a large Pb-scatterer peak at about 2.3 Å, with less intense peaks from outer atomic shell contributions between 2.80−4.30 and 4.00−6.10 Å. Manceau et al. (1996; ref *21*) suggested that the intensity of the outer shell peaks may correspond to the degree of structural order surrounding a Pb atom, and that peaks of low or weak amplitude indicate a variety of structural environments and greater structural disorder around the central Pb atom. The low intensity of the second and third shell contributions in the FTs of the current study may be similarly interpreted. Experimental Pb EXAFS data were modeled using a number of different scatterers in the outer shells. The best fits for each grain-size fraction are reported in Table 2. The quality of the fit is determined using the R and chi-squared (χ^2) values. The short EXAFS k-range for the 1000−500 μm fraction means that fitting of the grain-size data can only be justified to the first shell. By contrast, fitting of the experimental data for the 250−125 μm fraction was justified to three shells (Table 2). For the two finest fractions the best statistically justified fits for the experimental data were attained with a two shell model, with a first shell of lighter scatterers such as O atoms at approximately 2.3 Å and a second outer shell of heavier scatterers (e.g., Pb) at approximately 5.0 and 4.6 Å (63−38 and <38 μm, respectively). For the 250−125 and 63−38 μm samples modeling the data with scatterers of either Fe or Pb in the outermost shells gives comparable R-value. Consideration of the χ^2-values, however, allows differentiation between the two fits and for both of these grain-size fractions, the best fit involves Pb (or atoms of similar backscattering properties) in the third and second shell, respectively, and only these models are shown in Table 2 and Figure 3.

The fitted Pb−O distance and low coordination numbers of the first shell data are consistent with those reported for Pb(II)-sorbed species on goethite and hematite (*19*). There is also similarity to Pb(II)-sorbed species on aluminum oxides (*18*), the Mn-oxide birnessite (*11*) and feldspar and mica (*22*). Within the limits of error (±0.04 Å) for Pb first shell scattering distances, similarities were noted between the modeled EXAFS data and the Pb-O distances of a number of phosphate phases, including pyromorphite ($Pb_5[Cl(PO_4)_3]$), previously identified in contaminated soils and sediments (*10, 23*). The Pb−O distances in the EXAFS models for the Manchester RDS are consistent with Pb−O distances reported for Pb oxides (tetragonal PbO, Pb tetroxide, Pb_3O_4, Pb_2O_3, and Pb_2O) (*24−28*).

The EXAFS-derived second shell Pb−Fe backscattering distance (3.27 Å) for the 250−125 μm fraction is comparable to second shell Pb−Fe separations reported for Pb sorption complexes on Fe oxides, and in particular goethite and hematite (*19, 29, 30*). The derived Pb−Fe distance is also consistent with Pb edge-sharing complexes, but too short for corner sharing sites (≥3.9 Å) and conversely, too long for face-sharing adsorption (2.9−3.1 Å) (*19, 30*). Comparison of the EXAFS with second neighbor coordination number and Pb−Fe distances determined for Pb−FeO_6 octahedra complexes (*30*) suggests that Pb sorbed species in the Manchester RDS are likely to bind as bidentate or tridentate edge-sharing complexes.

The Pb EXAFS data for second shell scatterers show similarities between the 63−38 μm and the Pb−Pb scattering distances recorded for tetragonal PbO and Pb dioxide (PbO_2) (*27, 28*). Although no comparability is apparent for the oxysalts $PbCrO_4$, $Pb(NO_3)_2$ and $PbSO_4$ (*31−33*), similarity is noted between the experimental Pb−Pb scattering distances and the basic carbonate phase plumbonacrite (*34*). For the <38 μm fraction close similarities are evident between the experimental Pb−Pb scattering distances and data presented for $PbCrO_4$ (*38*).

The third shell Pb−Pb scattering distances for the 250−125 μm fraction show clear comparability with tetragonal PbO, plumbonacrite, and $PbCl_2$ (*28, 34, 35*).

Comparison of XANES dData, EXAFS Models, and SEM Observations. EXAFS modeled Pb−O distances of 2.29−2.32 Å for the first shell in all grain-size fractions support the presence of Pb species sorbed on goethite. This is corroborated by the Pb−Fe second shell scatterer distance of 3.27 Å in the 250−125 μm grain-size fraction, XANES fitting and the SEM-detected presence of Fe oxide grains within the RDS. EXAFS fitting only indicates $PbCrO_4$ in the <38 μm fraction, despite linear combination XANES fitting suggesting it exists in all of the size fractions analyzed. The XANES analysis suggests that $PbCl_2$ contributes significantly to the linear combination fit of the 250−125 μm fraction. While no confirmatory Pb−Cl scattering distances of 2.87−3.08 Å (*35*) are discerned in the EXAFS fits, the third shell Pb−Pb distances reported for the best fit may reflect $PbCl_2$ in the RDS matrix, and this is further indicated by the presence of Pb−Cl grains in SEM observations. Similarly, second shell Pb−Pb modeled distances are consistent with a basic Pb carbonate phase, as indicated in linear combination XANES fitting.

Implications for Speciation Assessment. Previous authors, using chemically based selective sequential extraction

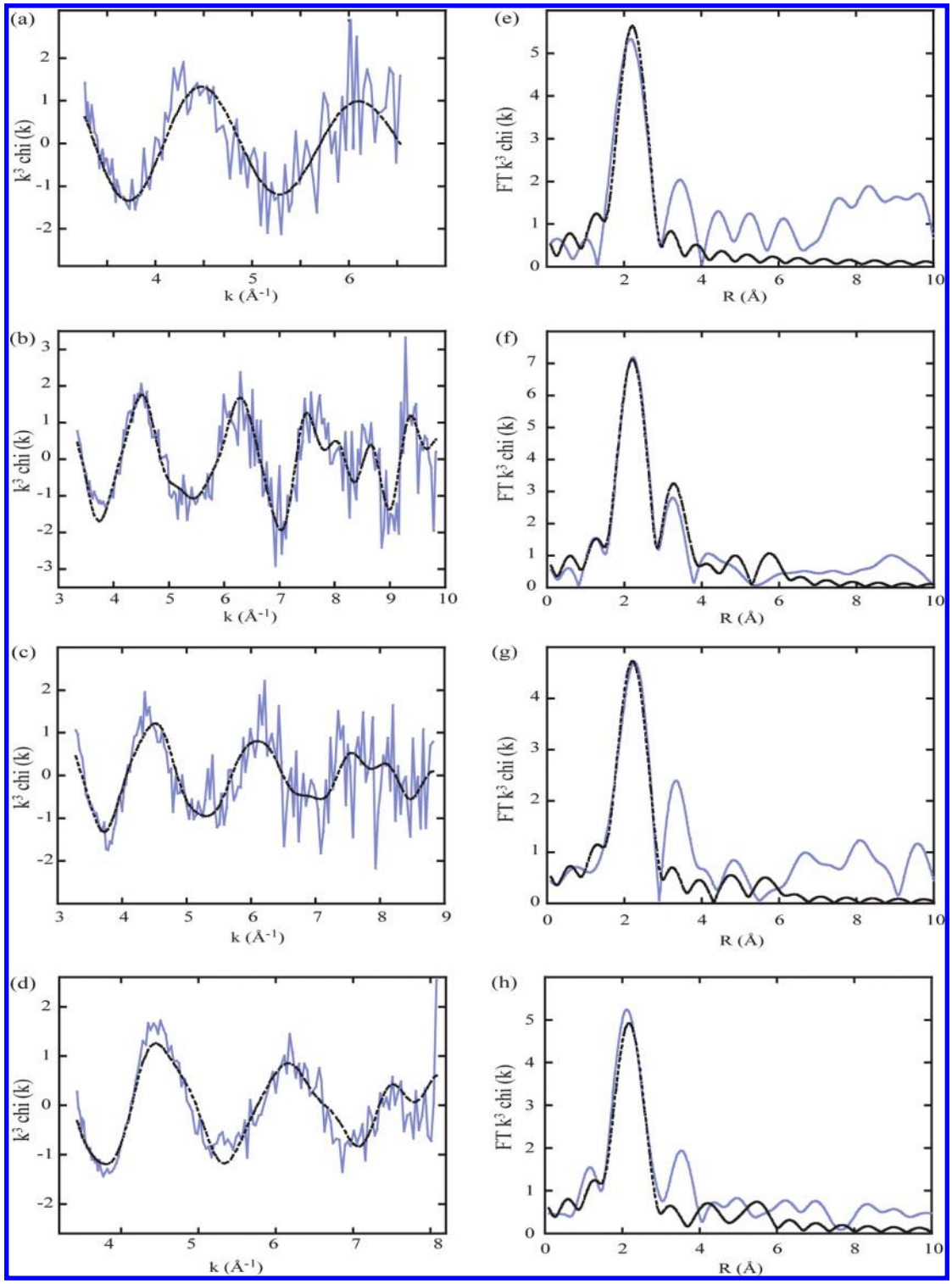

FIGURE 3. EXAFS spectra (a−d) and Fourier transform (e−h) (phase corrected for first shell scatterers; for comparative purposes *k*-range set at 8 Å) of Pb in Manchester RDS; theoretical fit using absolute goodness of fit (χ^2) parameters (Table 2) is given by dashed black lines. EXAFS experimental results are given by solid lines.

techniques (SSE), including data from samples from the site studied in this paper, have proposed the carbonate fraction and the Fe/Mn oxide fraction to be important hosts for Pb (*36*, *37*). The contributions made by Pb-sorbed on goethite to the theoretical XANES fits of four grain-specific fractions would appear to confirm that Fe oxides play an influential role in the speciation of Pb in the RDS matrices. Similar agreement between conventional Pb speciation data and our XANES analysis is not evident for the carbonate fraction. Carbonate ligands are only seen to be a significant component in the 63−38 μm fraction in the Manchester RDS. It is likely that discrepancies between the two approaches arise due to overestimation of Pb in the carbonate phase due to non-selectivity of the reagents used in the SSE (*38*). Consequently, the amount of Pb partitioned in the carbonate phase may be overestimated. $PbCl_2$ and $PbCrO_4$ phases are not recognized in the SSE schemes, highlighting the limitations of chemical approaches.

Implications for Environmental Quality and Human Health. We have shown that EXAFS and XANES analysis can

TABLE 2. Parameters Used in Fitting Pb L_{III}-EXAFS Data for the 1000-500 μm, 250−125 μm, 63−38 μm, and <38 μm Grain-Size Fractions of the Manchester RDS[a]

grain-size (μm)	k_{max}	shell	scatterer	*N*	distance *R* (Å)	$2\sigma^2$ (Å^2)	*R* factor	χ^2
1000−500	6.50	1	O	2	2.32	0.022	58.22	202.16
250−125	9.80	1	O	2	2.29	0.015		
		2	Fe	1	3.27	0.016		
		3	Pb	3	5.08	0.010	49.13	26.51
63−38	8.80	1	O	2	2.32	0.027		
		2	Pb	2	5.03	0.018	61.35	46.76
<38	8.00	1	O	2	2.30	0.027		
		2	Pb	2	4.64	0.013	39.94	24.52

[a] Notes: N is the EXAFS derived coordination number (±15% for inner shells; ±25% outer shells). R is the interatomic distance in Angstroms (±0.04 Å for inner shells; ±0.05 Å outer shells). $2\sigma 2$ is the Debye-Waller factor (±15% for inner shells; ±25% outer shells), a measure of both the static disorder of absorber-scatterer distances and the thermal motion between absorber and scatterer. R-factor is the least squares residual from fitting the theoretical fit to the experimental spectrum. $\chi 2$ is the measure of the absolute goodness of fit. The independent variables refined were a single energy correction Ef, and two variable (r and $2\sigma 2$) for each shell in the final.

characterize the Pb-phases within urban road dusts. Such data allow for better assessment of Pb mobility in the urban environment and provide novel data to inform assessments of potential human health impacts. The environmental and human health impacts of the Pb-phases depend largely on their solubility, which in turn depends on the mineral form, particle size, encapsulation by other phases, solution pH, Eh and inorganic and organic composition, and the action of biological agents (*39, 40*). For example, the Pb-bearing iron oxides that are dominant in most of the RDS size-fractions (Table 1) will be relatively insoluble and stable in oxic road surface environments (*41*), but will likely dissolve in anoxic urban gulley pots (*42*), sewers, and aquatic sediments, releasing their sorbed Pb. The detected $PbCrO_4$, $PbSO_4$, $PbCl_2$, and $Pb_5[Cl(PO_4)_3]$ (Table 1) have low solubility at most pH and Eh ranges typical of urban environments (ref *39*, and references therein), and thus will likely persist. By contrast, PbO and Pb acetate are soluble in most natural waters (*39, 43*), and will likely transform to other phases, possibly releasing Pb. As solubility increases with decreasing particle size, the PbO and Pb acetate in the <38 μm fraction, which forms 12.9 and 13.4% of the total Pb, respectively (Table 1), will likely be the most susceptible to dissolution.

Humans are exposed to RDS through inhalation and ingestion pathways. Uptake through the former generally involves very fine-grained fractions, herein represented by the <38 μm size fraction. Insoluble phases in urban air particulates have been shown to have the highest inflammatory impacts in lungs (*44*), but the water-soluble fractions can also disrupt lung function (*45*). All of the Pb-phases identified in the Manchester RDS therefore have the potential to have adverse effects when inhaled. The relatively insoluble $PbCrO_4$, for example, has been associated with cancers of the respiratory tract (*44, 46*). If ingested, the Pb-phases will pose a risk if they are dissolved during passage through the digestive tract. Based on their solubility (e.g., ref *39*), the predicted order of bioaccessibility of the RDS phases in all grain-size fractions is PbO ≥ Pb acetate > $(PbCO_3)_2 \cdot Pb(OH)_2$ > $PbCl_2$ > $PbSO_4$ > $PbCrO_4$ > Pb-goethite > $Pb_5[Cl(PO_4)_3]$, but this will depend on the pH and composition of the digestive fluids. In vitro bioaccessibility tests representing the respiratory tract (*47*) and stomach (*48*) on these Pb-phases and on bulk Pb-bearing RDS are required to give more detailed information on the potential uptake of Pb and risk to human health through the inhalation and ingestion pathways.

Acknowledgments

This work was funded through an EPSRC research studentship award to JEB (GR/P00666/01) and a CCLRC beamtime award (ref 45087), which are both gratefully acknowledged. We wish to acknowledge the use of the EPSRC's Chemical Database Service at Daresbury. We thank the station scientist Bob Bilsborrow for his assistance during the data collection at Daresbury.

Supporting Information Available

Table S1 (Pb concentration and mass-loading for all grain-sizes studied), Table S2 (the full elemental breakdown for all grainsizes), and Figure S1 (comparison of XANES experimental spectra and linear combination modeling). This material is available free of charge via the Internet at http://pubs.acs.org.

Literature Cited

(1) UNFPA. *State of the World population 2007: Unleashing the Potential of Urban Growth*; United Nations: New York, 2007.
(2) Taylor, K. G.; Owens, P. N. Sediments in urban river basins: a review of sediment-contaminant dynamics in an environmental system conditioned by human activities. *J. Soils Sediments.* **2009**, *9*, 281–303.
(3) Papanikolaou, N. C.; Hatzidaki, E. G.; Belivanis, S.; Tzanakakis, G. N.; Tsatsakis, A. M. Lead toxicity update: a brief review. *Med. Sci. Monit.* **2005**, *11*, RA329–RA336.
(4) Duggan, M. J.; Williams, S. Lead-in-dust in city streets. *Sci. Total Environ.* **1977**, *7*, 91–97.
(5) Biggins, P. D. E.; Harrison, R. M. Chemical speciation of lead compounds in street dusts. *Environ. Sci. Technol.* **1980**, *14*, 336–339.
(6) Kirpichtchikova, T. A.; Manceau, A.; Spadini, L.; Panfili, F.; Marcus, M. A.; Jacquet, T. Speciation and solubility of heavy metals in contaminated soil using X-ray microfluorescence, EXAFS spectroscopy, chemical extraction, and thermodynamic modeling. *Geochim. Cosmochim. Acta* **2006**, *70*, 2163–2190.
(7) Funasaka, K.; Tojo, T.; Katahira, K.; Shinya, M.; Miyazaki, T.; Kamiura, T.; Yamamoto, O.; Moriwaki, H.; Tanida, H.; Takaoka, M. Detection of Pb-LIII edge XANES spectra of urban atmospheric particles combined with simple acid extraction. *Sci. Total Environ.* **2008**, *403*, 230–234.
(8) Charlesworth, S. M.; Lees, J. A. The distribution of heavy metals in deposited dusts and sediments, Coventry, UK. *Environ. Geochem. Health* **1999**, *21*, 97–115.
(9) Schwertmann, U., Cornell, R. M. *Iron Oxides in the Laboratory: Preparation and Characterization.* VCH Publishers: New York, 1991.
(10) Cotter-Howells, J. D.; Champness, P. E.; Charnock, J. M.; Pattrick, R. A. D. Identification of pyromorphite in mine-waste contaminated soils by ATEM and EXAFS. *Eur. J. Soil Sci.* **1994**, *45*, 393–402.
(11) Manceau, A., Marcus, M. A., Tamura, N. Quantitative speciation of heavy metals in soils and sediments by synchrotron X-ray techniques. In *Reviews in Mineralogy and Geochemistry*; Fenter, P. A., Rivers, P. A., Sturchio, M. I., Sutton, N. C. S. R., Eds; Mineralogical Society of America: Washington DC, 2002; Vol. 49.

(12) Welter, E.; Calmano, W.; Mangold, S.; Tröger, L. Chemical speciation of heavy metals in soils by use of XAFS spectroscopy and electron microscopical techniques. *Freseniuś J. Anal. Chem.* **1999**, *364*, 238–244.
(13) Gurman, S. J.; Binsted, N.; Ross, I. A rapid, exact curved-wave theory for EXAFS calculations. *J. Phys. C: Solid State Phys.* **1984**, *17*, 143–151.
(14) Binsted, N. *EXCURV98*; STFC Daresbury Laboratory: Daresbury, UK, 1998.
(15) Hedin, L.; Lundqvist, S. Effects of electron-electron and electron-phonon interactions on the one-electron states of solids. *Solid State Phys. Adv. Res. Appl.* **1969**, *23*, 1–181.
(16) Binsted, N.; Strange, R. W.; Hasnain, S. S. Constrained and restrained refinement in EXAFS data analysis with curved wave theory. *Biochemistry* **1992**, *31*, 12117–12125.
(17) Taylor, K. G.; Robertson, D. J. Electron microbeam analysis of urban road-deposited sediment, Manchester, UK: Improved source discrimination and metal speciation assessment. *Appl. Geochem.* **2009**, *24*, 1261–1269.
(18) Bargar, J. R.; Brown, G. E., Jr.; Parks, G. A. Surface complexation of Pb(II) at oxide-water interfaces: I. XAFS and bond valence determination of mononuclear and polynuclear Pb(II) sorption products on aluminium oxides. *Geochim. Cosmochim. Acta* **1997a**, *61*, 2617–2637.
(19) Bargar, J. R.; Brown, G. E., Jr.; Parks, G. A. Surface complexation of Pb(II) at oxide-water interfaces: II. XAFS and bond valence determination of mononuclear Pb(II) sorption products and surface functional groups on iron oxides. *Geochim. Cosmochim. Acta* **1997b**, *61*, 2639–2652.
(20) Waychunas, G. A.; Apted, M. J.; Brown, G. E., Jr. X-ray K-edge absorption spectra of Fe minerals and model compounds: Near-edge structure. *Phys. Chem. Minerals* **1983**, *10*, 1–9.
(21) Manceau, A.; Boisset, M.-C.; Sarret, G.; Hazemann, J.-L.; Mench, M; Cambier, Ph.; Prost, R. Direct determination of lead speciation in contaminated soils by EXAFS spectroscopy. *Environ. Sci. Technol.* **1996**, *30*, 1540–1552.
(22) Farquhar, M. L.; Vaughan, D. J.; Hughes, C. R.; Charnock, J. M.; England, K. E. R. Experimental studies of the interaction of aqueous metal cations with mineral substrates: Lead, cadmium, and copper with perthitic feldspar, muscovite, and biotite. *Geochim. Cosmochim. Acta* **1997**, *61*, 3051–3064.
(23) Krivovichev, S. V.; Burns, P. C. Crystal chemistry of lead oxide phosphates: Crystal structure of $Pb_4O(PO_4)_2$, $Pb_8O_5(PO_4)_2$ and $Pb_{10}(PO_4)_6O$. *Z. Kristallogr.* **2003**, *218*, 357–365.
(24) Ferrari, A. Il sottossido di biombo. *Gazz. Chim. Ital.* **1926**, *56*, 630–637.
(25) Bouvaist, J.; Weigel, D. Sesquioxyde de Plomb, Pb_2O_3. I. Détermination da la structure. *Acta Crystallogr., Sect. A: Cryst. Phys., Diffr., Theor. Gen. Crystallogr.* **1970**, *26*, 501–510.
(26) Gavarri, J.-R.; Weigel, D. Oxydes de plomb. I. Structure cristalline du minium Pb_3O_4, à température ambiante (293K). *J. Solid State Chem.* **1975**, *13*, 252–257.
(27) Hill, R. J. The crystal structures of lead dioxides from the positive plate of the lead/acid battery. *Mater. Res. Bull.* **1982**, *17*, 769–784.
(28) Baldinozzi, G.; Raulot, J-M; Petricek, V. Reinvestigation of the Incommensurate Structure of alpha-PbO. *Mater. Res Soc. Symp. Proc.* **2002**, *755*, 465–470.
(29) Manceau, A.; Charlet, L.; Boisset, M. C.; Didier, B.; Spadini, L. Sorption and speciation of heavy metals on hydrous Fe and Mn oxides. From microscopic to macroscopic. *Appl. Clay Sci.* **1992**, *7*, 201–223.
(30) Ostergren, J. D.; Trainor, T. P.; Bargar, J. R.; Brown, G. E., Jr.; Parks, G. A. Inorganic ligand effects on Pb(II)sorption to goethite (α- FeOOH). I. Carbonate. *J. Colloid Interface Sci.* **2000**, *225*, 466–482.
(31) Sahl, K. Verfeinerung der kristallstruktur von cerussit, $PbCO_3$. *Z. Kristallogr.* **1974**, *139*, 215–222.
(32) Quareni, S.; de Pieri, R. A three-dimensional refinement of the structure of crocoite, $PbCrO_4$. *Acta Crystallogr.* **1965**, *19*, 287–289.
(33) Nowotny, H.; Heger, G. Structure refinement of lead nitrate. *Acta Crystallogr., Sect. C: Cryst. Struct. Commun.* **1986**, *C42*, 133–135.
(34) Krivovichev, S. V.; Burns, P. C. Crystal chemistry of basic lead carbonates II. Crystal structure of synthetic 'plumbonacrite'. *Mineral. Mag.* **2000**, *64*, 1069–1075.
(35) Nozik, Y. Z.; Fykin, L. E.; Muradyan, L. E. Crystal structure of contunnite $PbCl_2$ determined more precisely by application of the neutron diffraction method. *Kristallografiya* **1976**, *21*, 76–79.
(36) Harrison, R. M.; Laxen, D. P. H.; Wilson, S. J. Chemical Associations of lead, cadmium, copper, and zinc in street dusts and roadside soils. *Environ. Sci. Technol.* **1981**, *15*, 1378–1383.
(37) Robertson, D. J.; Taylor, K. G.; Hoon, S. R. Geochemical and mineral characterisation of urban sediment particulates, Manchester UK. *Appl. Geochem.* **2003**, *18*, 269–282.
(38) La Force, M. J.; Fendorf, S. Solid-phase iron characterization during common selective sequential extractions. *Soil Sci. Soc. Am. J.* **2000**, *64*, 1608–1615.
(39) Ruby, M. V.; Schoof, R.; Brattin, W.; Goldade, M.; Post, G.; Harnois, M.; Mosby, D. E.; Casteel, S. W.; Berti, W.; Carpenter, M.; Edwards, D.; Cragin, D.; Chappell, W. Advances in evaluating the oral bioavailibility of inorganics in soil for use in human health risk assessment. *Environ. Sci. Technol.* **1999**, *33*, 3697–3705.
(40) Dubbin, W. E.; Ander, E. L. Influence of microbial hydroxamate siderophores on Pb(II) desorption from α-FeOOH. *Appl. Geochem.* **2003**, 1751–1756.
(41) Schwertmann, U. Solubility and dissolution of iron oxides. *Plant Soil* **1991**, *130*, 1–25.
(42) Morrison, G. M.; Revitt, D. M.; Ellis, J. B. The gully pot as a biochemical reactor. *Water Sci. Technol.* **1995**, *31*, 229–236.
(43) Giordano, T. H. Anglesite ($PbSO_4$) solubility in acetate solutions: The determination of stability constants for lead acetate complexes to 85°C. *Geochim. Cosmochim. Acta* **1989**, *53*, 359–366.
(44) Jalava, P. I.; Salonen, R. O.; Pennanen, A. S.; Happo, M. S.; Penttinen, P.; Hälinen, A. I.; Sillanpää, M.; Hillamo, R.; Hirvonen, M.-R. Effects of solubility of urban air fine and coarse particles on cytotoxic and inflammatory responses in RAW 264.7 macrophage cell line. *Toxicol. Appl. Pharmacol.* **2008**, *229*, 146–160.
(45) Zhou, H.; Kobzik, L. Effect of concentrated ambient particles on macrophage phagocytosis and killing of *Streptococcus pneumoniae*. *Am. J. Respir. Cell Mol. Biol.* **2007**, *36*, 460–465.
(46) Frenzel-Beyme, R. Lung cancer mortality of workers employed in chromate pigment factories; a multicentric European epidemiological study. *J. Cancer Res. Clin. Oncol.* **1983**, *105*, 183–188.
(47) Beeston, M. P.; van Elteren, J. T.; Selih, V. S.; Fairhurst, R. Characterization of artifically generated PbS aerosols and their use within a respiratory bioaccessibility test. *Analyst* **2010**, *135*, 351–357.
(48) Morman, S. A.; Plumlee, G. S.; Smith, D. B. Application of in vitro extraction studies to evaluate element bioaccessibility in soils from a transect across the United States and Canada. *Appl. Geochem.* **2009**, *24*, 1454–1463.

ES903737K